NANO LETTERS

pubs.acs.org/NanoLett

Surface Plasmons and Singularities

Yu Luo,* J. B. Pendry, and Alexandre Aubry

The Blackett Laboratory, Department of Physics, Imperial College London, London SW7 2AZ, U.K.

ABSTRACT We apply the conformal transformation technique to study systematically a variety of singular plasmonic structures, including two-dimensional sharp edges, rough surfaces, and nanocrescents. These structures are shown to exhibit two distinct features. First, different from a planar metallic surface, the surface plasmon excitations on the examined structures have a lower bound cutoff at a finite frequency; second, the electric field diverges below a critical frequency even when metallic losses are considered. For rough surfaces and open-crescent nanostructures, the influence of the structure shapes on the absorbance characteristics is also discussed. Our analysis gives a unique insight into the light capture process on singular structures and holds the promise of detection of single molecules and greatly enhanced nonlinear effects.

KEYWORDS Surface plasmons, singular structures, transformation optics, field enhancement, broadband absorption

Surface plasmon-polaritons (SPPs) allow for the manipulation of light and electronic signals at subwavelength scale.[1,2] Various geometries have been proposed and experimentally studied to demonstrate subwavelength confinement and nanofocusing of surface plasmons, among which surfaces with sharp edges or other types of singularities supporting strongly localized plasmon-polariton modes are of particular interest.[3−21] Research on these plasmonic structures has already resulted in the development of practical nanosystems capable of concentrating and delivering light energy to nanoscale regions,[3−14] and important future practical applications of those devices are strongly dependent on further theoretical advances in this area. Indeed, current theoretical studies on this problem are mostly limited to numerical methods, which have limited value in studying singularities. Some analytical studies have been made by some researchers, showing that surface plasmon polaritons propagating toward the singularity of the structures are slowed down, and the energy is highly confined to the vicinity of the singularity.[7,12] However, to the best of our knowledge some important issues, such as the divergent features of the structure and the influence of source location on the field enhancement, have not been discussed yet. Therefore, analytical approaches that can systematically investigate these singular structures are still in great demand.

Transformation optics[22,23] enables the investigation of a complicated plasmonic system by first analyzing the properties of a simple well understood canonical structure. Recently, this concept has been applied to design broadband light harvesting devices. Two simple structures, a pair of kissing cylinders and a crescent with touching claws have been considered to illustrate the general approach.[14] In fact, when extended to much more general cases where the vertex angles (as defined in the latter part of the letter) of the singular structures are nonzero, numerous new capabilities will emerge. In this letter, we use the method of transformation optics to study quantitatively the surface plasmon modes supported by a variety of singular structures and to systematically investigate their plasmonic properties in terms of the vertex angle. Different from the two devices discussed in ref 14, singular plasmonic structures with a nonzero vertex angle are generally found to exhibit a cutoff behavior and a divergent feature. The analytical results show that beyond a cutoff frequency, the electric field diverges at the vertex (singularity) of the structure even when the material is highly dissipative. This divergent feature then disappears above a critical frequency; the electric field vanishes as surface plasmons propagate toward the vertex, whereas a considerable field enhancement is still expected along the metal surface. Specifically, for metallic wedge/groove structures, we have found that the field enhancement becomes more and more sensitive to the source location as the frequency increases. For open crescents and rough surfaces, a unique absorbance behavior is observed. The important features above are not necessarily limited to structures discussed in this letter, and the proposed strategy may help guide future research on other singular nanostructures.

Our discussion starts with a line dipole array embedded in periodic metallic films, as shown in Figure 1a1,a2. Each metallic layer has a thickness d_3, and repeats in the y direction with a period d. Each element of the dipole array is assumed to have a dipole moment $\vec{p} = p_x\hat{x} + p_y\hat{y}$ with an induced potential

$$-\phi_{\text{in}} = \frac{1}{2\pi\varepsilon_0}\frac{xp_x + (y + md)p_y}{x^2 + (y + md)^2} \qquad (1)$$

where m is the index associated with the dipole located at $x = 0$, $y = md$. Then by applying a conformal mapping $z' = a\exp(2\pi z/d)$ (where $z = x + iy$, $z' = x' + iy'$), a metallic

* To whom correspondence should be addressed y.luo09@imperial.ac.uk.

Received for review: 07/16/2010
Published on Web: 09/14/2010

DOI: 10.1021/nl102498s | *Nano Lett.* **2010,** *10,* 4186–4191

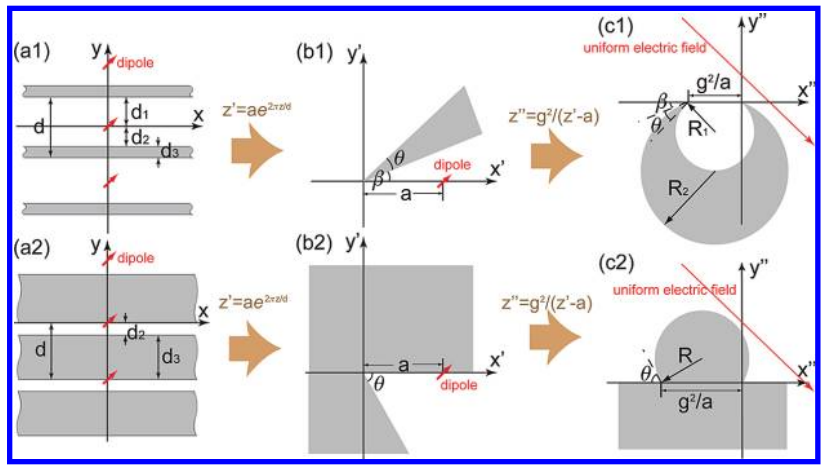

FIGURE 1. The schematic of the coordinate transformations. (a1),(a2) Periodic metallic thin films support surface plasmons that couple to a dipole array, transporting energy to infinity. The thickness of each metallic slab is d_3. Each element of the dipole array is located in vacuum with a distance d_1 to the upper adjacent slab, d_2 to the bottom adjacent slab (in (a2), $d_1 = 0$). And $d = d_1 + d_2 + d_3$ is the period of the metallo-dielectric structures; the conformal transformation $z' = a\exp(2\pi z/d)$ maps the configuration in (a1)/(a2) to a metallic wedge (b1)/V-shaped metallic groove (b2) excited by a single line dipole, where the energy is transported to infinity as well as the vertex of the structure; Finally, under the singular transformation $z'' = g^2/(z' - a)$, the wedge/groove-like structure in (b1)/(b2) are converted to a metallic crescent (c1)/metallic rough surface (c2). The single dipole source in (b1) and (b2) is mapped to a uniformed electric field E''_{inc} in (c1) and (c2).

wedge (Figure 1b1) and a V-shaped metallic groove (Figure 1b2) are obtained. In this process a singularity is created at the origin in z'. The vertex angle of the wedge or groove is denoted as θ ($\theta = 2\pi d_3/d$ for wedges; $\theta = 2\pi(d_1 + d_2)/d$ for grooves), and $\beta = 2\pi d_1/d$ represents the angular distance between the dipole and metal surface. The line dipole array (with each element at the position $z = 0, z = \pm id, z = \pm 2id...$) is mapped to a single line dipole located at $z' = a$ with the incident potential taking the form

$$-\phi'_{in} = \frac{1}{2\pi\varepsilon_0}\frac{(x' - a)p'_x + y'p'_y}{(x' - a)^2 + y'^2} \tag{2}$$

where $p'_x = (2\pi a/d)p_x$ and $p'_y = (2\pi a/d)p_y$ are the strength of the line dipole along x' and y' direction, respectively.

Next, another singular transformation $z'' = g^2/(z' - a)$ maps the wedge or groove to a crescent-shaped structure or convex rough surface (a cylinder overlapped with a semi-infinite slab). And the two charges comprising the dipole in z' are transformed to near infinity in z'', giving rise to an uniform electric field

$$E''_{inc} = \frac{(\hat{x}p'_x - \hat{y}p'_y)}{2\pi\varepsilon_0 g^2} = \frac{a(\hat{x}p_x - \hat{y}p_y)}{\varepsilon_0 d g^2} \tag{3}$$

We can also see from Figure 1c1,c2 that there are two singularities ($z'' = 0$ and $z'' = -g^2/a$) in both structures. It is worth pointing out that the crescent depicted in Figure 1c1 is different from the one discussed in ref 14 since there is a gap between the two claw tips of the crescent, allowing for some unique characteristics (demonstrated later).

In all the following discussions, we shall assume that the dimensions of the structures are sufficiently small compared with the wavelength of the probe light (e.g., a and $g^2/a < 50$ nm). Thus, we can neglect radiative effects decoupling the electric and magnetic fields and consider the electrostatic limit for *P*-polarized fields. In this case, the dielectric properties of the structures remain unchanged under conformal mappings, and the uniform electric field can be considered as a good approximation to plane wave illumination.[14] Because of the form invariance of Laplace's equation, the electrostatic potential is preserved $\phi(x,y) = \phi'(x',y') = \phi''(x'',y'')$, enabling us to calculate the field strength in the transformed geometries. Thus solving the tractable periodic slabs problem gives solutions to the problems of metallic wedges/grooves, crescent structures, and rough surfaces.

By considering periodic boundary conditions, the solution to the infinite periodic metallic slabs problem can easily be obtained, and the dispersion of surface plasmon excitations can be found from the condition that scattering coefficients diverge (a detailed derivation is provided in Supporting Information[24])

$$e^{2\alpha}(e^{|k|(d_1+d_2)} - e^{|k|d_3})^2 - (e^{|k|(d_1+d_2+d_3)} - 1)^2 = 0 \tag{4}$$

where

$$\alpha = \ln[(\varepsilon - 1)/(\varepsilon + 1)] \tag{5}$$

Solving eq 4 gives two bounded surface plasmon modes with symmetric and antisymmetric profiles of the tangential

DOI: 10.1021/nl102498s | *Nano Lett.* **2010,** *10,* 4186–4191

electric field E_x.[1] The symmetric (or even) mode spans the frequency range $[\omega_c, \omega_{sp}]$, while the antisymmetric (or odd) mode spans the range $[\omega_{sp}, \omega'_c]$. Here, ω_{sp} denotes the surface plasma frequency (where $\mathrm{Re}\{\varepsilon(\omega_{sp})\} = -1$); ω_c and ω'_c are the lower and upper bound cutoff frequencies determined by the following equations

$$\mathrm{Re}\{\varepsilon(\omega_c)\} = -\frac{d_1 + d_2}{d_3},\ \mathrm{Re}\{\varepsilon(\omega'_c)\} = -\frac{d_3}{d_1 + d_2},\ \text{when } d_1 + d_2 > d_3 \quad (6a)$$

$$\mathrm{Re}\{\varepsilon(\omega_c)\} = -\frac{d_3}{d_1 + d_2},\ \mathrm{Re}\{\varepsilon(\omega'_c)\} = -\frac{d_1 + d_2}{d_3},\ \text{when } d_1 + d_2 < d_3 \quad (6b)$$

where $\varepsilon(\omega_c)$ and $\varepsilon(\omega'_c)$ represent the permittivity of the metal at ω_c and ω'_c, respectively. Because of their different propagation distances, the odd mode is often termed a long-range SPP in the literature, while the even mode is related to a short-range SPP.[1]

The spectrum of surface plasmon modes in a single metallic slab system has a lower bound cutoff at zero frequency and an upper bound cutoff at the bulk plasma frequency.[1] However, eqs 6a and 6b indicate that when the number of metallic films increases to infinity, the hybridization of surface plasmons on each interface of the slabs will create two band gaps respectively at the lower and higher frequency range, resulting in a nonzero lower bound cutoff and an upper bound cutoff below the bulk plasma frequency. Consequently, the transformed singular structures (shown in Figure 1b1,b2,c1,c2) exhibit similar behavior with a lower bound cutoff frequency ω_c and an upper bound cutoff frequency ω'_c determined by

$$\mathrm{Re}\{\varepsilon(\omega_c)\} = \frac{\theta - 2\pi}{\theta},\ \mathrm{Re}\{\varepsilon(\omega'_c)\} = \frac{\theta}{\theta - 2\pi} \quad (7)$$

Equation 7 shows that the two cutoff frequencies of a singular structure only depend on the vertex angle θ.

The optical parameters of noble metals[25] indicate that the odd mode (namely, the surface plasmon excitation above the surface plasma frequency) is relatively narrow-band. (e.g., for silver with a surface plasma frequency $\omega_{sp} = 880$ THz and a bulk plasma frequency $\omega_p = 910$ THz, the bandwidth of the odd mode is at most 30 THz.) Therefore, in the following discussions we shall focus on the frequency range below the surface plasma frequency, where only the even mode needs to be considered. To understand further the surface plasmon modes supported by the transformed singular structures, we calculate the scattered field strength for the metallic wedge/groove

$$\left|\bar{E}'^{\mathrm{scatt}}\right| = \underbrace{\frac{\left|f_{\alpha,\theta}\right|}{8\pi^2\varepsilon_0 a\rho'}}_{\text{Compression factor}} \times \underbrace{\left(\frac{\rho'}{a}\right)^{\mathrm{Im}\{f_{\alpha,\theta}\}\mathrm{sgn}(a-\rho')/\pi}}_{\text{Dissipation loss}} \times \sqrt{Ae^{2\mathrm{Re}\{f_{\alpha,\theta}\}\varphi'/\pi} + Be^{-2\mathrm{Re}\{f_{\alpha,\theta}\}\varphi'/\pi}}, \quad (8)$$

where $\rho' = (x'^2 + y'^2)^{1/2}$; A and B are coefficients given in ref 24. Here the time dependence $e^{i\omega t}$ is implicit. $f_{\alpha,\theta}$ is a complex number determined by θ and α (α is defined by eq 5) through the following equation

$$e^{\alpha}\sinh[(1 - \theta/\pi)f_{\alpha,\theta}] = \sinh f_{\alpha,\theta} \quad (9)$$

The first factor on the right side of eq 8 is a result of the distortion of space under the transformation, while the second and third factors represent the propagation of surface plasmon mode along the radial ρ' and angular φ' directions, respectively. The surface plasmon mode is excited at the position $\rho' = a$ and propagates to infinity as well as to the vertex of the structure. Normally, we expect that the surface wave amplitude decreases along its propagating direction due to dissipation in the material. Nevertheless, the situation is different here, since the field can be enhanced at the vertex of the structure. This phenomenon can be understood by checking eq 8. Although the metallic losses will cause a decrease of the field by a factor $\rho'^{\mathrm{Im}\{f_{\alpha,\theta}\}/\pi}$ (see the second factor on the right side of eq 8) as the surface wave propagates to the vertex ($\rho' = 0$), the compression of surface plasmons would enhance the electric field by ρ'^{-1} (see the first factor on the right side of eq 8) as $\rho' \to 0$. Thus, whether the electric field is enhanced or decreased at the vertex is determined by the values of the two factors. Hence the critical condition is deduced as

$$\mathrm{Im}\{f_{\alpha,\theta}\} = \pi \quad (10)$$

Considering the first order approximation of $f_{\alpha,\theta}$, eq 10 can be simplified to

$$\mathrm{Im}\{\alpha\} = \theta \quad (11)$$

At the frequency that satisfies eq 11, the electric field at the vertex converges to a nonzero value. Accordingly, we refer to it as the critical frequency ω_0. Below ω_0 (where $\mathrm{Im}\{\alpha\} < \theta$), the electric field diverges at the vertex of the structure, even if the metal is highly dissipative. In contrast, above ω_0 (where $\mathrm{Im}\{\alpha\} > \theta$), the electric field decreases and finally vanishes as surface plasmons propagate toward the vertex.

DOI: 10.1021/nl102498s | Nano Lett. 2010, 10, 4186–4191

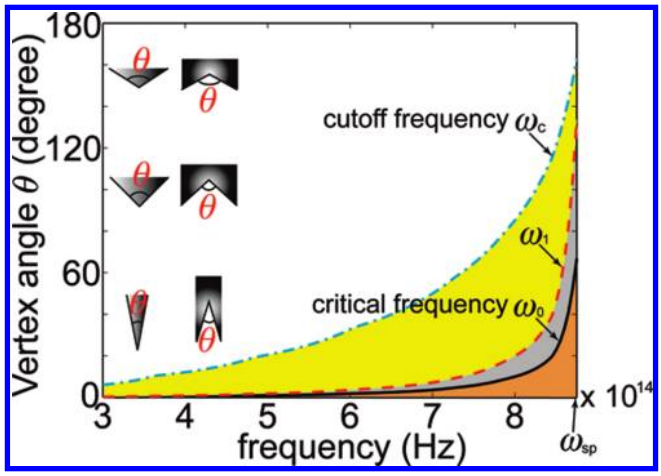

FIGURE 2. For a certain vertex angle, there are three crucial frequencies. The black solid line denotes the critical frequency ω_0 where $\mathrm{Im}\{\alpha\} = \theta$; the red dashed line corresponds to ω_1 where $2\,\mathrm{Im}\{\alpha\} = \theta$; and the blue dot dashed line is the cutoff frequency ω_c where $\mathrm{Re}\{\varepsilon\} = 1 - 2\pi/\theta$. In the range $[\omega_c, \omega_1]$, both the electric field and total Raman signal in a volume diverge; in the range $[\omega_1, \omega_0]$, the electric field blows up at the vertex, while the total Raman signal in a volume converges to a finite value; in the range $[\omega_0, \omega_{sp}]$, the electric field vanishes at the vertex.

The above analysis is summarized in Figure 2, which shows the relation between the plasmonic properties of the metallic wedge and the vertex angle θ. The metal is assumed to be silver, and the permittivity is taken from experimental results.[25] The cutoff frequency ω_c and the critical frequency ω_0 are denoted by the blue dash-dot line and black solid line, respectively. From the figure we can see that the frequency band $[\omega_c, \omega_0]$ increases as the vertex angle θ decreases. Also, it gets relatively broadband for small θ angles (e.g., when $\theta = 9°$, $\omega_0 - \omega_c = 450$ THz). Here we emphasize that numerical methods could never get accurate results in this frequency band since dealing with the divergence of electric fields requires infinitely dense meshes.

Despite the infinite field strength below the critical frequency, a detailed calculation shows that the total power in a volume always converges to a finite value.[24] In other words, the divergence of the electric field does not conflict with the conservation of energy. Another relevant quantity from the perspective of single molecule detection is the Raman signal (defined as the power density scattered by molecules on the surface of the structure). To a first approximation, it is proportional to $|E'_{\mathrm{scatt}}|^4$. Interestingly, our analytical results show that the total Raman signal in a volume diverges under the condition $2\,\mathrm{Im}\{f_{\alpha,\theta}\} < \pi$ (or $2\,\mathrm{Im}\{\alpha\} < \theta$). We refer to the frequency at which $2\,\mathrm{Im}\{\alpha\} = \theta$ as ω_1 (the red dashed line in Figure 2). It is worth noticing that ω_1 is slightly different from the critical frequency ω_0. In the frequency range $[\omega_1, \omega_0]$ (the gray region in Figure 2) the electric field blows up at the vertex while the total Raman signal integrated over volume still remains finite. On the other hand, when $\omega_c < \omega < \omega_1$ (the yellow region in Figure 2), both the electric field and total Raman signal diverge. It should be pointed out that in practical designs, a perfect wedge can never be fabricated. In addition, the nonlocal properties of ε encountered at small length scales[26] will also prevent the electric field from increasing to infinity. However, our approach does indicate that a sharp wedge is still capable of enhancing the field to the atomic field scale. Therefore, closer to the vertex, a molecule will experience a considerably larger power density. This property is potentially applicable in the optical characterization of single molecules.[13,15,27]

Another interesting phenomenon associated with the wedgelike structures is the influence of the source location on the surface plasmon excitations. To illustrate this point, Figure 3 depicts the calculated electric field distribution of a metallic wedge with a vertex angle of 9°. A line dipole is placed at two different angular positions around the vertex. Figure 3a,b shows the electric field distributions at 350 THz (the cutoff frequency where $\varepsilon = -38.49 + 3.33i$). We can see that most of the energy is confined to the vicinity of the vertex, irrespective of where the source is located. Figure 3c,d corresponds to a frequency of 800 THz (the critical frequency where $\varepsilon = -3.07 + 0.79i$). A considerable field enhancement (up to 100) can be observed along the edge of the structure when the dipole is placed close to the metal surface (Figure 3c). In contrast, the coupling to surface plasmons is very weak ($|E'_{\mathrm{scatt}}| \sim 10^{-3}$) if the dipole is located on the other side of the vertex (Figure 3d). The field distributions for 875 THz (close to the surface plasmon frequency, where $\varepsilon = -1.09 + 0.51i$), shown in Figure 3e,f, confirm this trend. At this frequency, the energy is confined around the point where the surface plasma is excited ($\rho' = a$) and the influence of the dipole position is even more drastic; the field enhancement increases to 800 when the dipole is placed close to the metal surface (Figure 3e) whereas the coupling to surface plasmons becomes extremely low ($|E'_{\mathrm{scatt}}| \sim 10^{-9}$) in the other configuration (Figure 3f). In other words, as the frequency increases, the surface plasmon excitations get more and more sensitive to the position of the dipole, which is a remarkable property for potential sensing applications.

Since the vertex angle is preserved after conformal transformations, the crescents[15−18] and rough surfaces[19,20] are found to exhibit similar properties (e.g., similar cutoff and divergent features) with the metallic wedgelike structures. Further analysis is made by calculating the absorption cross sections of these structures. Since the total energy is conserved under transformations, the power absorbed by the nanostructure in the transformed coordinate system z'' is equivalent to the power dissipated by the dipole in the original geometry z.[14] The calculated absorption cross sections σ_a^x and σ_a^y associated with x'' and y'' polarizations are depicted in Figure 4. The top three panels of Figure 4 show the results for the crescent with $\theta = 9°$ as a function of β and frequency (θ and β are defined in Figure 1c1). Different from the crescent case discussed in ref 14 where only one continuous and broadband absorbance is observed, Figure

DOI: 10.1021/nl102498s | Nano Lett. 2010, 10, 4186–4191

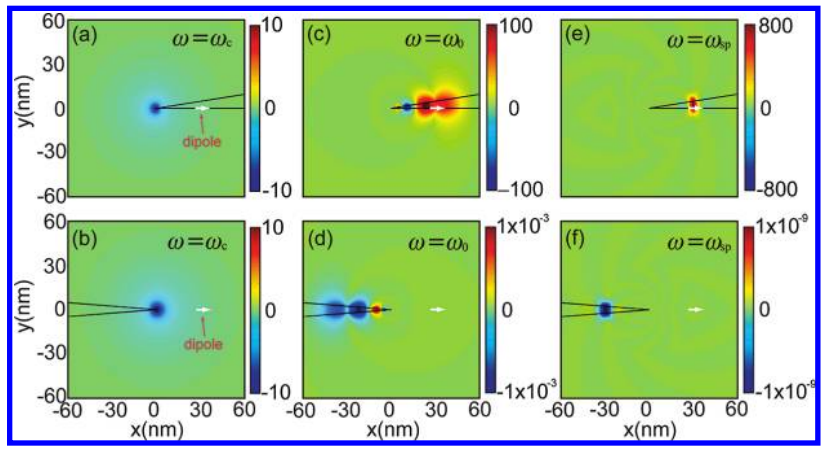

FIGURE 3. The normalized electric field for a 9° silver wedge with x-polarized dipole sources placed at different positions around the vicinity of the vertex. Panels in the three columns from left to right correspond to the cutoff frequency 350 THz, the critical frequency 800 THz, and the surface plasma frequency 875 THz, respectively. These field distributions have been normalized by the field magnitude that would be obtained at the vertex in absence of the metallic wedge.

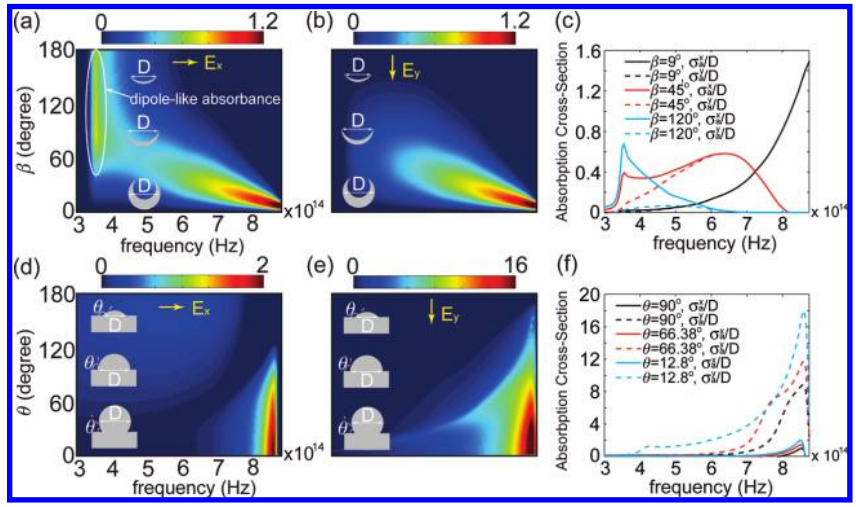

FIGURE 4. Absorption cross sections for crescent (top panels) and convex (bottom panels) rough surfaces. The left column corresponds to the horizontal polarized illumination and the middle column corresponds to the vertical polarized illumination. For the purpose of a clearer observation, we plot the absorption cross-section as a function of the frequency for structures with different β- (or θ) angles in the right column. Here the solid lines denote the horizontal polarized cases and the dashed lines denote the vertical polarized cases.

4a indicates that the crescents with untouched claws exhibit two distinct absorbance bands for the x'' polarization, one close to the cutoff frequency ω_c, the other close to the surface plasma frequency ω_{sp}. Near ω_c, surface plasmons are highly concentrated at the singularities of the two claws. Hence, the cutoff frequency absorbance is associated with a dipole-like resonance, and the equivalent dipole moment is proportional to the distance between the two tips of the crescent. As shown in Figure 4a, this resonance strongly depends on the angle β; the cutoff frequency absorbance dominates for large β-angles (or large distance between the two crescent tips), and vanishes as β decreases. On the other hand, the absorbance band close to ω_{sp} corresponds to the overall structure resonance. It is relatively broadband, but only appears for a narrow range of small β-angles. When β increases, the hybridization of the surface plasmon with the tip resonance results in a red shift of the absorbance band.

Moving on to Figure 4b, we find the cutoff frequency absorbance disappears, since the dipole-like resonance is suppressed for y-polarized illumination. Figure 4c depicts the absorption cross sections for three special cases (where $\beta =$ 9, 45, and 120°, respectively). In particular, when $\beta = 45°$, a large and continuous absorption cross-section over a wide band spectrum can be observed.

The bottom panels of Figure 4 correspond to the results for convex rough surfaces. The absorption cross-section increases as the vertex angle θ decreases, and the maximum always occurs at the surface plasma frequency ω_{sp}. Apart from that, Figure 4f indicates that the Raman intensity is significantly enhanced for y-polarized illumination. This is due to the coupling between the cylinder and the semi-infinite plane plasmons, similar to the case discussed in ref 21.

DOI: 10.1021/nl102498s | Nano Lett. 2010, 10, 4186–4191

To conclude, we have established analytical relationships between a canonical two-dimensional metallo-dielectric system and a variety of singular plasmonic structures. The divergence conditions of the electric field, total power, and total Raman signal as well as the influence of the source location and incident wave polarization on the surface plasmon excitations have been discussed in detail. Our approach can be generalized to investigate some other complicated plasmonic systems containing singularities and therefore may provide guidance in a number of practical applications with metallic nanostructures.

Acknowledgment. Y.L. acknowledges the Lee family scholarship for financial support. This work was partly supported by the European Community project PHOME (Contract No. 213390).

Supporting Information Available. Dispersion of the surface plamon excitation, calculation of the field distribution, total power, and total Raman signal in a volume, and absorption cross-sections of open crescents and rough surfaces. This material is available free of charge via the Internet at http://pubs.acs.org.

REFERENCES AND NOTES

(1) Maier, S. A. *Plasmonics: Fundamentals and Applications*; Springer, New York, 2007.
(2) Gramotnev, D. K.; Bozhevolnyi, S. I. *Nat. Photonics* **2010**, *4*, 83–91.
(3) Novikov, I. V.; Maradudin, A. A. *Phys. Rev. B* **2002**, *66*, No. 035403.
(4) Bozhevolnyi, S. I.; Volkov, V. S.; Devaux, E.; Ebbesen, T. W. *Phys. Rev. Lett.* **2005**, *95*, No. 046802.
(5) Pile, D. F. P.; Ogawa1, T.; Gramotnev, D. K.; Okamoto, T.; Haraguchi, M.; Fukui, M.; Matsuo, S. *Appl. Phys. Lett.* **2005**, *87*, No. 061106.
(6) Moreno, E.; Rodrigo, S. G.; Bozhevolnyi, S. I.; Martín-Moreno, L.; García-Vidal, F. J. *Phys. Rev. Lett.* **2008**, *100*, No. 023901.
(7) Gramotnev, D. K. *J. Appl. Phys.* **2005**, *98*, 104302.
(8) Volkov, V. S.; Bozhevolnyi, S. I.; Rodrigo, S. G.; Martín-Moreno, L.; García-Vidal, F. J.; Devaux, E.; Ebbesen, T. W. *Nano Lett.* **2009**, *9*, 1278–1282.
(9) Maier, S. A.; Andrews, S. R.; Martín-Moreno, L.; García-Vidal, F. J. *Phys. Rev. Lett.* **2006**, *97*, 176805.
(10) Choi, H.; Pile, D. F.; Nam, S.; Bartal, G.; Zhang, X. *Opt. Express* **2009**, *17*, 7519–7524.
(11) Oulton, R.; Sorger, V.; Genov, D. A.; Pile, D. F. P.; Zhang, X. *Nat. Photonics* **2008**, *2*, 496–500.
(12) Stockman, M. I. *Phys. Rev. Lett.* **2004**, *93*, 137404.
(13) Angelis, F. D.; Das, G.; Candeloro, P.; Patrini, M.; Galli, M.; Bek, A.; Lazzarino, M.; Maksymov, I.; Liberale, C.; Andreani, L. C.; Fabrizio, E. D. *Nat. Nanotechnol.* **2010**, *5*, 67–72.
(14) Aubry, A.; Lei, D. Y.; Fernandez-Dominguez, A. I.; Sonnefraud, Y.; Maier, S. A.; Pendry, J. B. Plasmonic light harvesting devices over the whole visible spectrum. *Nano Lett.* **2010**, *10*, 2574–2579.
(15) Lu, Y.; Liu, G. L.; Kim, J.; Mejia, Y. X.; Lee, L. P. *Nano Lett.* **2005**, *5*, 119–124.
(16) Shumaker-Parry, J. S.; Rochholz, H.; Kreiter, M. *Adv. Mater.* **2005**, *17*, 2131–2134.
(17) Bukasov, R.; Shumaker-Parry, J. S. *Nano Lett.* **2007**, *7*, 1113–1118.
(18) Rochholz, H.; Bocchlo, N.; Kreiter, M. *New J. Phys.* **2007**, *9*, 53.
(19) Moskovits, M. *Rev. Mod. Phys.* **1985**, *57*, 783–826.
(20) García-Vidal, F. J.; Pendry, J. B. *Phys. Rev. Lett.* **1996**, *77*, 1163–1166.
(21) Wei, H.; Hao, F.; Huang, Y.; Nordlander, P.; Xu, H. X. *Nano Lett.* **2008**, *8*, 2497–2502.
(22) Ward, A. J.; Pendry, J. B. *J. Mod. Opt.* **1996**, *43*, 773–93.
(23) Pendry, J. B.; Schurig, D.; Smith, D. R. *Science* **2006**, *312*, 1780–1782.
(24) Please see Supporting Information for detailed derivations of the dispersion relation, field distribution, and absorption cross-section.
(25) Palik, E. D. *Handbook of Optical Constants of Solids*; Academic: New York, 1991; Vol. *II*.
(26) Lindhardt, J. Kgl. Danske Videnskab. Selskab, Mat.-Fys.; 1954, 28, No. 8.
(27) Schultz, S.; Smith, D. R.; Mock, J. J.; Schultz, D. A. *Proc. Natl. Acad. Sci. U.S.A.* **2000**, *97*, 996–1001.

DOI: 10.1021/nl102498s | *Nano Lett.* **2010,** *10,* 4186–4191